Chemical Physics Letters 714 (2019) 149–155

Contents lists available at ScienceDirect

Chemical Physics Letters

journal homepage: www.elsevier.com/locate/cplett

Research paper

Functionalized few-layered graphene oxide embedded in an organosiloxane matrix for applications in optical limiting

Surendra Maharjan[a,*], Kang-Shyang Liao[a], Alexander J. Wang[a], Zhuan Zhu[b], Kamrul Alam[c], Brian P. McElhenny[a], Jiming Bao[b], Seamus A. Curran[a]

[a] Institute for NanoEnergy, Department of Physics, University of Houston, Houston, TX 77204, USA
[b] Department of Electrical and Computer Engineering, University of Houston, Houston, TX 77204, USA
[c] Department of Materials Science and Engineering, University of Houston, Houston, TX 77204, USA

HIGHLIGHTS

- Graphene oxide (GO) is synthesized via chemical exfoliation of bulk graphite.
- Functionalized GO is incorporated in polymer matrix using a sol-gel process.
- Functionalized GO is significantly better optical limiter than its GO precursor.
- Nonlinear scattering and nonlinear absorption are the mechanisms responsible for optical limiting.

ARTICLE INFO

Keywords:
Graphene oxide
Organosiloxane
Sol-gel
Optical limiting
Z-scan

ABSTRACT

Few-layered graphene oxide is covalently functionalized with (3-Aminopropyl)triethoxysilane and incorporated into an organosiloxane matrix using a sol-gel technique. Nonlinear optical and optical limiting properties of functionalized few layered graphene oxide embedded in an organosiloxane matrix (f-GO/sol) are studied in the nanosecond regime at 527 nm. In a Z-scan study, f-GO/sol samples exhibit superior nonlinear optical and optical limiting responses in comparison to their graphene oxide precursor due to increased covalent crosslinking of graphene oxide and organosiloxane molecules. These significant improvements are attributed to the combined mechanisms of nonlinear absorption and nonlinear scattering, due to graphene-silica nanostructures and thermally-generated microplasmas.

1. Introduction

A practically uncountable number of applications for the laser across various fields has imposed a great challenge to protect human eyes and sensitive optical devices ever since its inception in 1960 [1–3]. Thereby it has become crucial to find an ideal optical limiter which attenuates intense laser beams while readily allowing transmittance for low-intensity light. Several optical limiting (OL) materials have been discovered and developed in recent years to meet this challenge, including organic dyes (e.g., phthalocyanines [4] and porphyrins [5]), organometallics, liquid crystals [6], microbiologically-formed tellurium nanorods [7], inorganic nanostructures [8], and carbon-based materials (e.g., carbon black [9], fullerenes [10,11] carbon nanotubes [10,12], and graphene [13,14]). Recently attention has shifted to graphene and its hybrids due to their excellent nonlinear optical (NLO) properties. Graphene is a two-dimensional π-conjugated system, exhibiting an unusual electronic structure with a linear dispersion of electrons. Interband optical transitions in graphene are independent over a broad range of light frequencies and depend only on the fine structure constant [15,16]; this makes graphene an excellent candidate for a broadband NLO material. However, limited processibilty due to the hydrophobic nature of graphitic materials is a challenge in the NLO materials development and research.

Graphene oxide (GO), a chemically exfoliated graphene derivative, consists of peripherally oxidized graphene sheets [17]. The peripheral functionalized groups open the possibility of interlinking GO with other nanoparticles, substrates, or functional groups to form hybrid materials. These hybrid GO materials have been shown to outperform pristine graphene in NLO applications [18,19]. Nonlinear scattering (NLS), nonlinear absorption (NLA), and the formation of a donor-acceptor

* Corresponding author.
E-mail address: smaharjan@uh.edu (S. Maharjan).

https://doi.org/10.1016/j.cplett.2018.11.007
Received 17 September 2018; Received in revised form 5 November 2018; Accepted 7 November 2018
Available online 08 November 2018
0009-2614/ Published by Elsevier B.V.

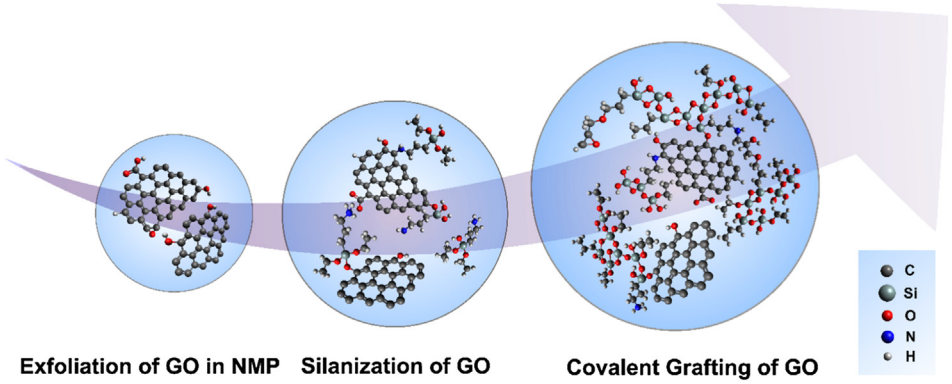

Fig. 1. Schematic diagram for the preparation of GO functionalized with APTES incorporated in an organosiloxane matrix (f-GO/sol).

system are vital mechanisms to realize efficient NLO behavior in GO hybrid materials [20,21].

This paper reports an effective and convenient method to prepare highly dispersed, functionalized GO in an organosiloxane matrix (f-GO/sol). GO was prepared by ultrasonication of graphite powder in N-methyl-2-pyrrolidone (NMP), and then was covalently functionalized via amination reactions of GO with (3-aminopropyl)triethoxysilane (APTES). Peripheral carboxylic acid groups of GO in an NMP environment react with the primary amine groups of APTES to form −CO−NH bonds [21–23], which are then reacted (hydrolyzed and polycondensed) with organosilane precursors to establish Si−O bonding [24]. The NLO and OL behaviors of GO and f-GO/sol of equal linear optical transmittance have been studied using a Q-switched nanosecond pulse laser.

2. Experimental section

2.1. Materials

Graphite powder (< 20 μm, synthetic), N-methyl-2-pyrrolidone (anhydrous, 99.5%, NMP) and (3-aminopropyl)triethoxysilane (APTES, 99%) were purchased from Sigma-Aldrich and used without further purification. The precursors to a commercially available organosilane solution was obtained from Integricote, Inc.

2.2. Preparation of graphene oxide

Solvent-based exfoliation of graphite into graphene oxide was carried out via ultrasonication of graphite in NMP, a highly polar organic solvent [25,26]. Layers of graphene in graphite are bound together by Van der Waals forces. The shearing force needed to break these bonds and hence exfoliate graphite into graphene is delivered by NMP and ultrasound waves [27]. Specifically, 20 g of graphite powder was added into 200 mL of NMP and the resulting mixture was sonicated for 2 h and then stirred for 22 h. This process was repeated for 3 days. An aliquot of the supernatant was used in preparing f-GO/sol samples. The concentration of GO in solution was determined to be ~17 mg/mL by evaporation of solvents.

2.3. Preparation of functionalized graphene/sol

To functionalize GO, 0.30 mL of APTES was added to 30 mL of GO suspension and stirred for 48 h. 6 mL of the resulting mixture was added to 100 mL of organosilane precursor solution (sol), then stirred and heated at 50 °C for 5 h. The final mixture was allowed to stir at room temperature for another 72 h.

2.4. Materials characterization

UV–vis spectra were recorded using an Ocean Optics 2000+ Spectrometer. A quartz cuvette with a path length of 1.0 cm was used for transmission measurements. The morphology of GO was studied using a Leo 1525 Field Emission Scanning Electron Microscope. A Thermo Nicolet NEXUS 670 Fourier Transform Infrared spectrometer was used to obtain FTIR spectra of sol samples. FTIR spectra of f-GO/sol samples were taken with a nanoIR2 (Anasys Instruments) atomic force microscope with simultaneous infrared spectral analysis. AFM topography images were also obtained using a nanoIR2 (Anasys Instruments). Thermogravimetric analysis was performed with a TA Instruments Q600 SDT thermogravimetric analyzer under an argon environment. The XPS spectra were obtained using a Physical Electronics Model 5700 XPS system. The Z-scan setup incorporated a Q-switched Nd:YLF laser (Coherent Evolution) with a wavelength 527 nm, delivering a repetition rate of 1 kHz and pulse width of 150 ns. A standard photodiode power sensor S121C (Si, 400–1100 nm, 500 mW, ThorLabs) was used to measure the laser power. The laser beam was tightly focused using a 150 mm focal length lens, and transmitted light was collected using a 35 mm focal length lens. Z-scan measurements were carried out at three different single pulse energies; 15, 30, and 60 μJ. A quartz cuvette with a path length of 1.0 cm was placed on a translational stage allowing sample movement along the z-direction. Negative z values refer to the position when the sample is in between the focusing lens and beam focus (z = 0), whereas positive z values refer to the position when the sample is in between beam focus (z = 0) and the detector.

3. Results and discussions

Chemically exfoliated GO flakes possess hydroxyl and carboxyl functional groups bound to peripheral carbon atoms. GO was initially functionalized with an amino group (APTES) to achieve covalently bonded GO and APTES via −CO−NH− bonding, followed by hydrolyzation and polycondensation of GO-APTES in the presence of sol precursors. Finally, GO-APTES is covalently connected to the organosiloxane matrix through Si−O bonding, effectively mitigating agglomeration of GO. The synthesis scheme for the covalent grafting of GO in an organosiloxane matrix is presented in Fig. 1.

Fig. 2a shows digital photographs of GO (left) and f-GO/sol (right), which exhibited excellent miscibility in the sol. Fig. 2b shows UV–visible transmission spectra of the two specimens. Matching linear optical transmittance of ~22% was maintained for both samples at a wavelength of 527 nm. The transmission spectrum shows a band at 230 nm for f-GO/sol and a broader band from 230 nm to 280 nm for GO, which is the characteristic peak of graphene materials [20,28]. It corresponds to the $\pi \rightarrow \pi^*$ transition of aromatic C−C bond [21]. A field emission scanning electron microscope (FESEM) image of GO is presented in

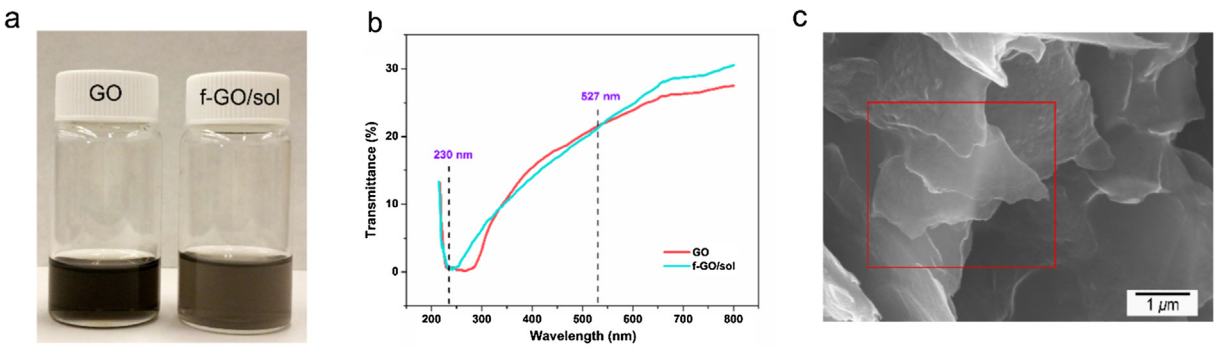

Fig. 2. (a) Digital photograph of GO and f-GO/sol. (b) UV–visible transmission spectra of GO and f-GO/sol (c) FESEM image of GO flakes.

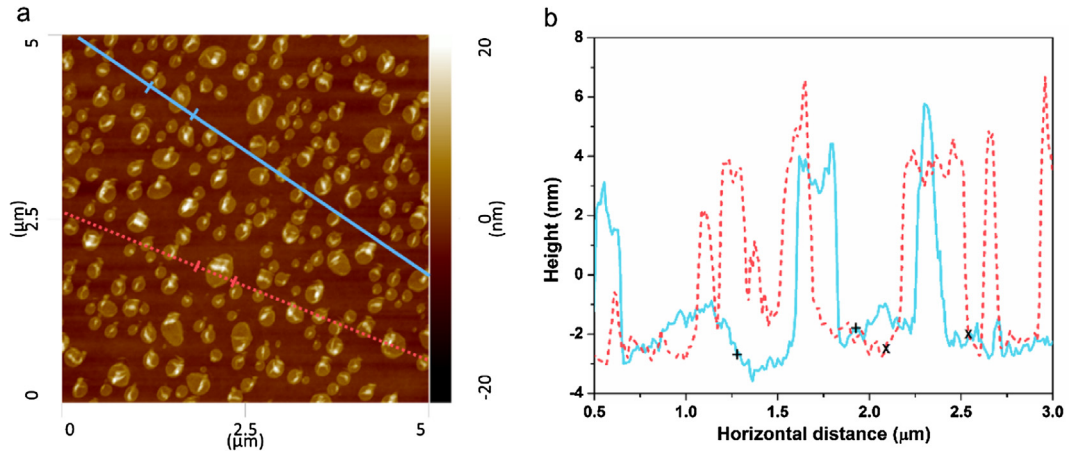

Fig. 3. (a) AFM topography image of f-GO/sol. (b) Height profile of GO platelets along the cyan (solid) and the red (dashed) lines drawn in Fig. 3a.

Fig. 2c. It exhibits typical graphene flakes with micrometer lateral dimensions. The flakes are so thin and transparent that the graphene flakes underneath are clearly visible.

An atomic force microscopy (AFM) topography image of as-prepared f-GO/sol is shown in Fig. 3a, which clearly shows the formation of highly dispersed GO platelets having submicron lateral dimensions. It is well known that single layer graphene on SiO_2 has an average thickness of ~1 nm [29,30]. Fig. 3(b) presents the height profile of graphene oxide platelets in f-GO/sol on a SiO_2 substrate. The height profile measurements along the cyan (solid) and the red (dashed) lines in Fig. 3a confirm the formation of few-layered GO platelets.

Characterization of the functional groups present in the sol components was done by FTIR spectroscopic measurements carried out at different reaction times under isothermal conditions at 40 °C; this data is presented in Fig. 4a. The characteristic peak at 958 cm^{-1} indicated the presence of the Si—O—Et stretching mode for an ethoxysilane, whereas absorption bands in the range 1030–1100 cm^{-1} are attributed to Si—O—Si stretching. Finally, the absorption band at 1193 cm^{-1} is attributed to Si—CH_2— stretching [31,32]. The sol-gel process for alkoxysilanes is a continuous chemical reaction that proceeds, at controllable rates, until polymerization via step-growth condensation reactions is complete. The chemical composition of sol is only minimally changed over time, which is verified by analysis of the FTIR data. The slight increase in peak height illustrates the high yield of functional groups corresponding to the particular wavenumbers. The FTIR spectrum of f-GO/sol presented in Fig. 4b shows characteristic absorption

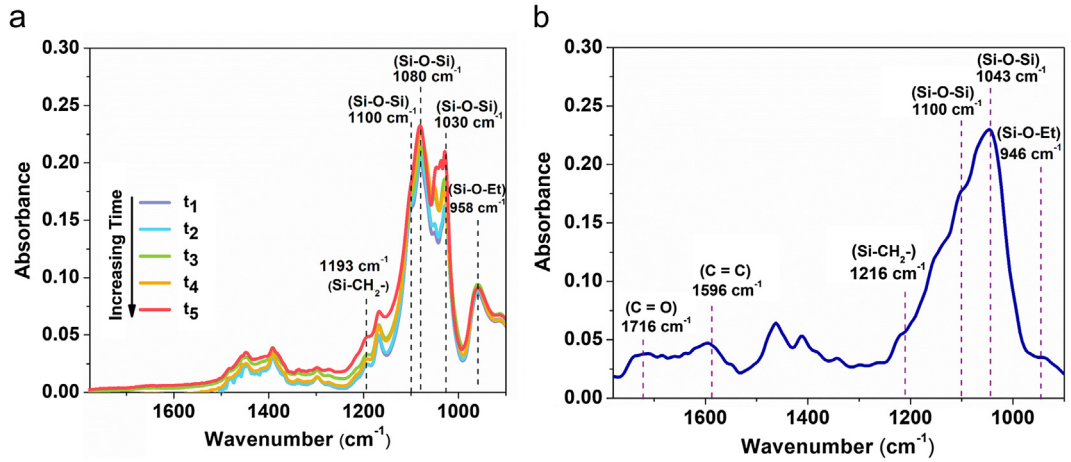

Fig. 4. (a) FTIR spectra of sol recorded at different times. (b) FTIR spectrum of f-GO/sol.

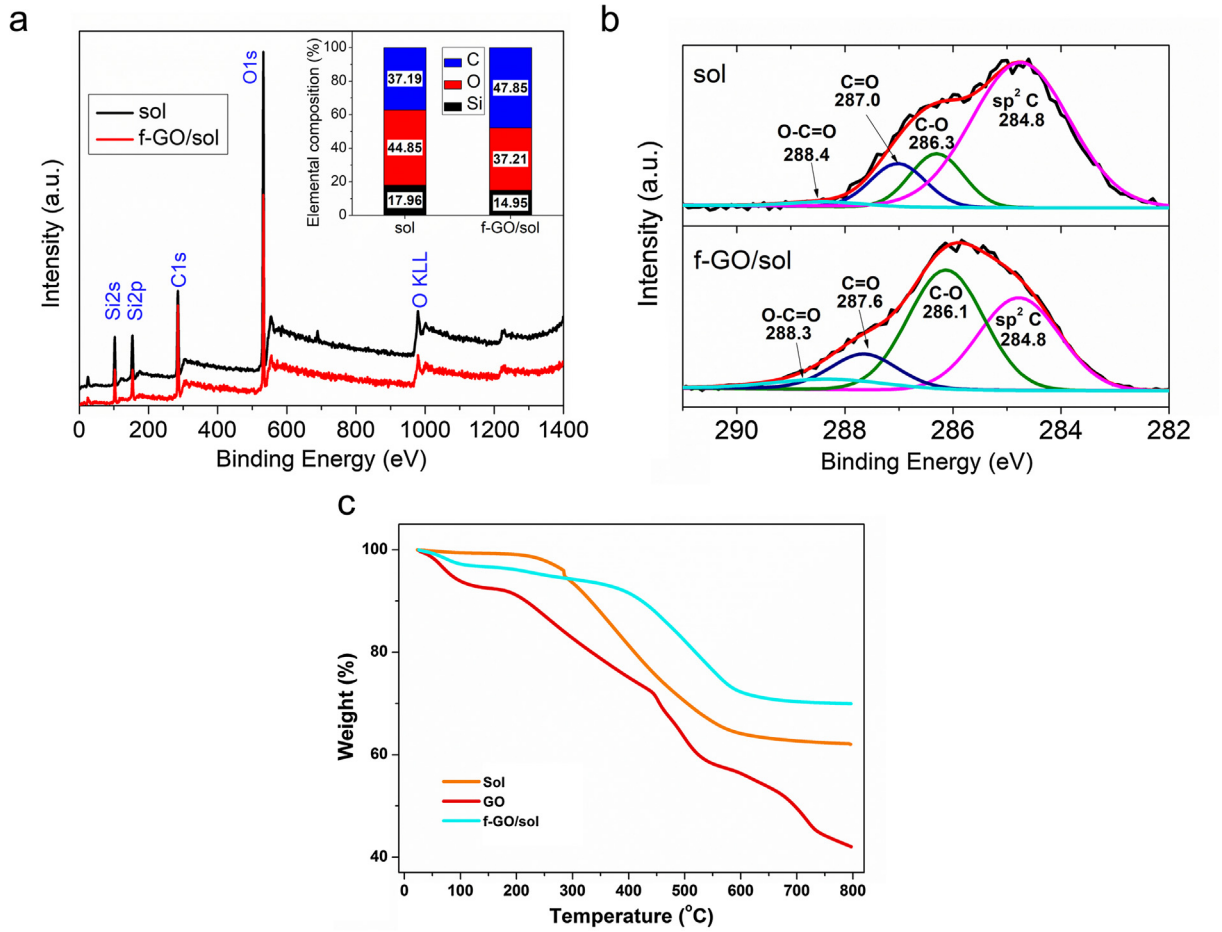

Fig. 5. (a) XPS survey scans of sol and f-GO/sol. Inset is the elemental composition (%) of sol and f-GO/sol. (b) Deconvoluted C 1s peaks for sol and f-GO/sol. (c) TGA thermograms of sol, GO, and f-GO/sol under an argon environment.

peaks also observed in the same wavenumber range as those present in the FTIR spectra of the sol. The peak at 946 cm^{-1} is due to Si—O—Et stretching, the bands in the range 1043–1100 cm^{-1} are attributed to Si-O-Si stretching. Similarly, the peak at 1216 cm^{-1} is assigned to Si—CH_2— stretching [32]. Two additional peaks at 1596 cm^{-1} and 1716 cm^{-1} are from C=C (graphitic domains) and C=O (carboxylic acid and carbonyl moieties), respectively [33,34].

X-ray photoelectron spectroscopy (XPS) characterization was carried out to identify the elemental composition of sol and f-GO/sol samples using a Physical Electronics Model 5700 XPS System. The XPS survey spectra show major peaks at Si 2s, Si 2p, C 1s, O 1s, and O KLL as shown in Fig. 5a. The O KLL corresponds to the energy of electron ejected from the atoms when O 1s state (K shell) is filled by an electron from L shell in conjunction with the ejection of an electron from an L shell. Fig. 5a inset presents the elemental composition of silicon, oxygen, and carbon in sol and f-GO/sol samples. In the sol sample, silicon is identified to be 17.96% while oxygen and carbon contents are 44.85% and 37.19% respectively, making the ratio of Si:O:C = 1:2.5:2.1. On the other hand, f-GO/sol sample constitutes 14.95% silicon, 37.21% oxygen, and 47.85% carbon that makes the ratio of Si:O:C = 1:2.5:3.2. It is evident that f-GO/sol contains a high proportion of carbon atoms in comparison to the sol sample while the ratio of silicon to oxygen stays the same; this effectively verifies a significant graphene presence in the f-GO/sol sample. Furthermore, Fig. 5b shows the deconvoluted C 1s XPS spectra of sol and f-GO/sol. The C 1s spectrum of sol contains four peaks at 284.8, 286.3, 287.0, and 288.4 eV corresponding to sp^2 hybridized carbon (72.1%), C—O (14.1%), C=O (11.9%), and O—C=O (1.8%) respectively. Likewise, C 1s spectrum of f-GO/sol also contains four spectra at similar binding energies, however, the intensities of the peaks are completely different compared to that of sol. The intensity of sp^2 carbon dramatically decreases from 72.1 to 36.4%, while the intensity of C—O bond increase from 14.1 to 44.4%, confirming the presence of significant amount of graphene oxide in f-GO/sol. The intensity of C=O remains approximately the same (12.9%), whereas O—C=O increases to 6.3% signifying the formation of additional carboxyl bonds [35,36].

To understand the thermal stability of the material system, thermogravimetric analysis (TGA) was performed at a heating rate of 20 °C/min under argon environment, where the decomposition pattern is presented in Fig. 5c. GO begins to thermally degrade as soon as it is heated. The initial ~7% weight loss below 110 °C is attributed to the removal of absorbed water molecules, followed by a significant weight loss above 200 °C due to pyrolysis of labile oxygen-containing functional groups. The stability of f-GO/sol gives the clear indication that most of the oxygen-containing functional groups are functionalized with APTES. For the f-GO/sol, the first significant weight loss is observed at ~370 °C, which is attributed to the loss of dopant molecules. As temperature increases the GO sample continues to lose weight, yielding only ~42% char residue at 800 °C. However, the total residual weights obtained at 800 °C for sol and f-GO/sol are 62% and 70%, respectively. These results indicate that f-GO/sol is more thermally stable than GO.

An open-aperture Z-scan technique was employed to study the NLO and OL properties of GO and f-GO/sol [37,38]. Generally, the mechanisms responsible for OL is comprised of NLA and NLS [6,38]. NLA is further divided into two-photon absorption (TPA) and excited state absorption (ESA), while free-carrier absorption also contributes significantly to NLA in the case of semiconductor nanoparticles or metal

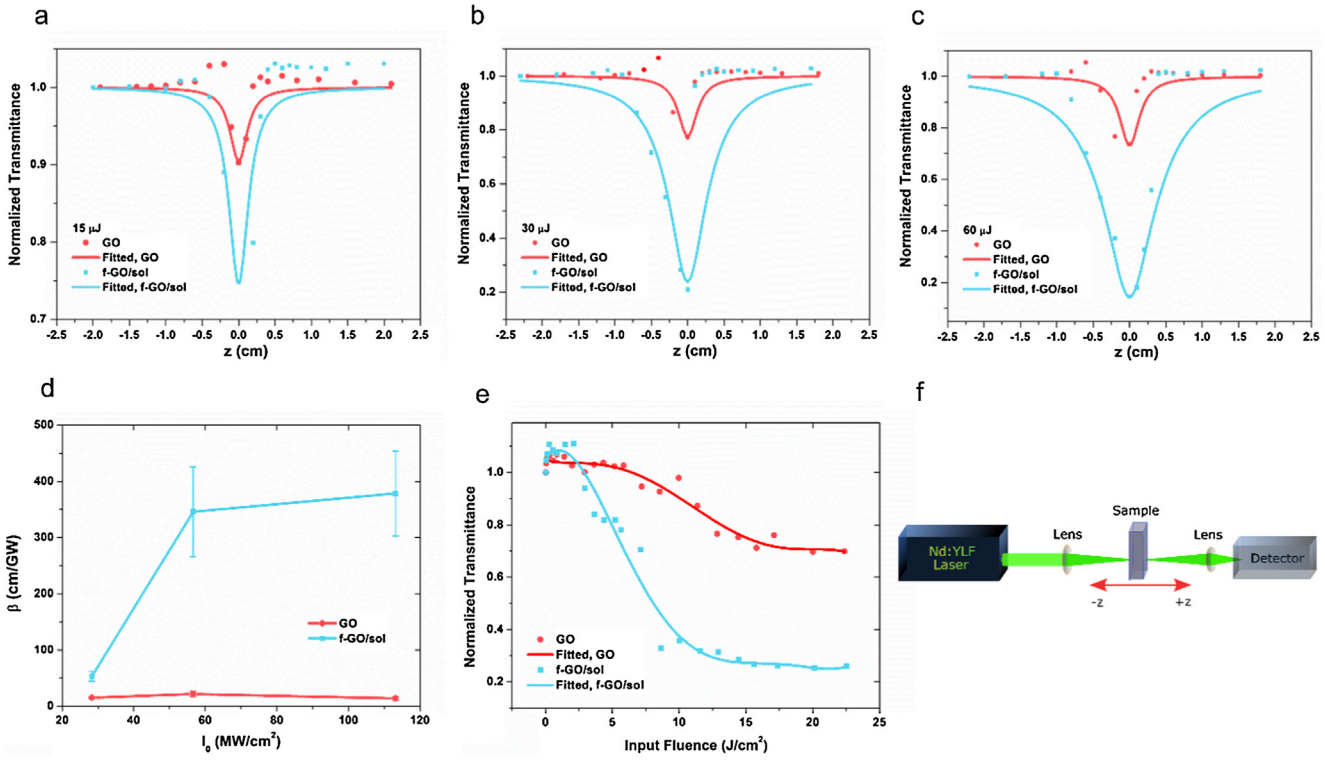

Fig. 6. Open-aperture Z-scan of GO and f-GO/sol at (a) ~28 MW/cm^2 (15 μJ), (b) ~56 MW/cm^2 (30 μJ), and (c) ~113 MW/cm^2 (60 μJ). (d) The effective nonlinear absorption coefficient plotted as a function of on-axis peak intensity. (e) Optical limiting responses of GO and f-GO/sol. (f) Schematic representation of open-aperture Z-scan setup.

nanocomposites [7]. NLS includes induced scattering centers that can arise from a number of physical phenomena, for example, the formation and expansion of thermally-induced solvent bubbles due to thermal energy transfer between nanoparticles and solvent, ionization of the nanoparticles themselves, or by thermal alteration of the solvent's refractive index [7,39]. The open-aperture Z-scan results of GO and f-GO/sol at mentioned pulse energies are shown in Fig. 6a–c. Both samples exhibit a symmetric valley of normalized transmittance about the focal point (z = 0) for all three different input energies, which is indicative of strong optical nonlinearity. However, no nonlinearity was observed for sol samples. The data at all three energies clearly show deeper valleys for the f-GO/sol than the GO alone, and verifies that the functionalization significantly enhances graphene's NLO properties. The normalized transmittance at 60 μJ reduces to ~0.15 at the focal point for f-GO/sol, while GO, having the same linear transmittance, exhibits a decrease to only ~0.75. The effective NLA coefficients, β, calculated from Z-scan results as a function of on-axis peak intensity, and the normalized transmittance versus laser input fluence are presented in Fig. 6d, e respectively. With an increase in input fluence, the normalized transmittance in f-GO/sol decreases more rapidly than in comparison to GO. A significant decrease in transmittance occurs at ~2.9 J/cm^2 for f-GO/sol, which is much lower than ~7.2 J/cm^2 for GO. At the maximum input fluence (22.4 J/cm^2) tested, the transmittance of GO reduces to 30% while about 80% reduction is observed in f-GO/sol. The outstanding OL performance of f-GO/sol is mainly due to much improved NLS and NLA phenomena as compared to GO [18,21,40–42]. Furthermore, the Z-scan measurements carried out with a 532 nm continuous wave laser (at an average power matching that of pulsed laser) produce a flat Z-scan profile. This verifies that the optical nonlinearity observed with nanosecond laser pulses is entirely due to optical nonlinear effects rather than thermal effects [43].

One of the most common nonlinear phenomena in nanomaterials, particularly graphitic, is NLS. Scattering from nanomaterials can greatly reduce the light intensity via dispersion into larger spatial dimensions, however, nanomaterials alone cannot effectively scatter the beam. Formation and growth of scattering centers from thermally induced solvent-bubbles and microplasmas, with sizes on the order of the incident wavelength, aid in the scattering process [7,8]. The scattering mechanism within f-GO/sol is primarily polymer bubble formation that occurs as a result of microplasma formation [44]. The possible mechanisms involved in the formation of nonlinear scattering centers in f-GO/sol include: (1) The absorption of incident photon energy by GO platelets that transfer the generated thermal energy to the surrounding organosiloxane host matrix, resulting in the formation and growth of gas bubbles, with GO as a nucleus, due to the large pressure difference across the vapor-solution interface. At the point when the dimension of gas bubble matches the wavelength of the incident photon, the incident beam is effectively scattered by bubble clouds, resulting in significant reduction in optical transmission. (2) The direct ionization of GO by the highly intense laser beam results in the formation of microplasmas in the host organosiloxane polymer matrix. The rapid growth of those microplasmas results in the establishment of scattering centers, followed by the significant attenuation of the intensity of the incident beam. On the other hand, NLA arises mainly due to TPA and ESA in graphene-based materials [45,46]. ESA is the dominant mechanism under resonant and near resonant excitations, whereas TPA dominates the NLO behavior under non-resonant excitation. Under some resonant excitation, both ESA and TPA may work synergistically leading to higher nonlinearities [47,48]. It has been found that the effective NLA coefficient, β, increases as the intensity of incident light increases in the case of ESA, while, β, stays almost constant for TPA [48].

To quantify the NLO parameters, we have simulated Z-scan data using Z-scan theory [7,37,38]. The normalized transmittance as a function of position, z, is given by

$$T_{\text{normalized}}(z) = \frac{Log_e[1 + q_o(z)]}{q_o(z)} \quad (1)$$

where $q_o(z) = q_{00}/[1+(z/z_0)^2$, z_0 is the diffraction length of the beam,

Table 1
Linear and nonlinear optical coefficients of GO and f-GO/sol at different input intensities of 527 nm excitation.

Material	Excitation intensity (MW/cm^2)	α_0 (cm^{-1})	β (cm/GW)	$Im\{\chi^{(3)}\}$ (10^{-11} esu)
GO	28	1.51	15.14 ± 1.85	6.68 ± 0.81
f-GO/sol			53.10 ± 8.82	19.93 ± 3.31
GO	56	1.51	21.65 ± 4.56	9.55 ± 2.01
f-GO/sol			345.92 ± 79.73	129.85 ± 29.85
GO	113	1.51	14.06 ± 3.03	6.20 ± 1.34
f-GO/sol			378.45 ± 75.57	142.06 ± 28.37

$q_{00}(z) = \beta I_0 L_{eff}$, β is the effective nonlinear absorption coefficient, I_0 is the on-axis peak intensity at the focal point ($z = 0$), $L_{eff} = [1 - \exp(-\alpha_0 l)]/\alpha_0$ is the effective thickness of the sample, α_0 is the linear absorption coefficient, and l is thickness of the sample. The effective imaginary third-order optical susceptibility $Im\{\chi^{(3)}\}$, which is directly related to, β, is given by

$$Im\{\chi^{(3)}\} = \frac{{n_0}^2 \varepsilon_0 c \lambda \beta}{2\pi} \quad (2)$$

where n_0 is the linear refractive index of the sample, ε_0 is the permittivity of free space, c is the speed of light, and λ is the wavelength of the incident light. We compare the OL performances of GO and f-GO/sol at various laser input intensities. Fig. 6d presents the variation in β with on-axis peak input intensity. A summary of NLO coefficients for GO and f-GO/sol having the same linear optical transmittance (~22% T at 527 nm) is presented in Table 1. β, inferred from Z-scan results, for f-GO/sol are 3, 16, and, 27 times greater than that of GO at 28, 56, and 113 MW/cm^2, respectively. Clearly β remains relatively constant within the intensity range tested for GO, which suggests that NLO behavior of GO is mainly due to NLS and TPA. In contrast, we observed a dramatic increase in β for f-GO/sol, implying that the origin of its enhanced NLO performance over GO is dominated by much improved NLS and ESA phenomena. ESA clearly dominates TPA as input intensity increases in f-GO/sol, which is confirmed by the increase of β.

4. Conclusions

Successful synthetization of covalently functionalized GO incorporated into an organosiloxane matrix (f-GO/sol) with a simple sol-gel technique has been achieved. The NLO and OL characteristics of GO and f-GO/sol materials were studied using the Z-scan technique at 527 nm with a 150 ns pulse laser. f-GO/sol exhibits significantly enhanced NLO and OL performance in comparison to its precursor, GO, with matching linear optical transmittance. The superiority in OL performance is attributed to the combined effect of improved NLA due to graphene-silica nanostructures, and NLS due to thermally-induced solvent bubbles. The excellent OL performance, along with its relatively simple and cost-effective synthesis, demonstrates that f-GO/sol is a promising optoelectronic and OL material. In addition, with mild thermal treatment, this hybrid material can form free-standing/supported solid films, rendering it an excellent candidate for laser protection devices.

Conflict of interest

The authors declare no competing financial interest.

Acknowledgements

We are grateful to Integricote, Inc., Houston, Texas for providing organosilane precursors. We would also like to thank Dr. Eoghan Dillon (Anasys Instruments) for kindly providing AFM images and FTIR studies.

References

[1] T.H. Maiman, Stimulated optical radiation in ruby, Nature 187 (1960) 493–494.
[2] C. Zheng, Y. Zheng, W. Chen, L. Wei, Encapsulation of graphene oxide/metal hybrids in nanostructured sol-gel silica ORMOSIL matrices and its applications in optical limiting, Opt. Laser Technol. 68 (2015) 52–59.
[3] M. Calvete, G.Y. Yang, M. Hanack, Porphyrins and phthalocyanines as materials for optical limiting, Synth. Met. 141 (2004) 231–243.
[4] J.J. Doyle, J. Wang, S.M. O'Flaherty, Y. Chen, a. Slodek, T. Hegarty, L.E. Carpenter II, D. Wöhrle, M. Hanack, W.J. Blau, Nonlinear optical performance of chemically tailored phthalocyanine–polymer films as solid-state optical limiting devices, J. Opt. A Pure Appl. Opt. 10 (2008).
[5] W. Blau, H. Byrne, W.M. Dennis, J.M. Kelly, Reverse saturable absorption in tetraphenylporphyrins, Opt. Commun. 56 (1985) 25–29.
[6] L.W. Tutt, T.F. Boggess, A review of optical limiting mechanisms and devices using organics, fullerenes, semiconductors and other materials, Prog. Quant. Electron. 17 (1993) 299–338.
[7] K.S. Liao, J. Wang, S. Dias, J. Dewald, N.J. Alley, S.M. Baesman, R.S. Oremland, W.J. Blau, S.a. Curran, Strong nonlinear photonic responses from microbiologically synthesized tellurium nanocomposites, Chem. Phys. Lett. 484 (2010) 242–246.
[8] J. Wang, W.J. Blau, Inorganic and hybrid nanostructures for optical limiting, J. Opt. A Pure Appl. Opt. 11 (2009) 024001.
[9] K. Mansour, M.J. Soileau, E.W. Van Stryland, Nonlinear optical properties of carbon-black suspensions (ink), J. Opt. Soc. Am. B. 9 (1992) 1100.
[10] K.S. Liao, J. Wang, D. Früchtl, N.J. Alley, E. Andreoli, E.P. Dillon, A.R. Barron, H. Kim, H.J. Byrne, W.J. Blau, S.A. Curran, Optical limiting study of double wall carbon nanotube-Fullerene hybrids, Chem. Phys. Lett. 489 (2010) 207–211.
[11] L.W. Tutt, A. Kost, Optical limiting performance of C60 and C70 solutions, Nature 356 (1992) 225–226.
[12] J. Wang, K.-S. Liao, D. Früchtl, Y. Tian, A. Gilchrist, N.J. Alley, E. Andreoli, B. Aitchison, A.G. Nasibulin, H.J. Byrne, E.I. Kauppinen, L. Zhang, W.J. Blau, S.a. Curran, Nonlinear optical properties of carbon nanotube hybrids in polymer dispersions, Mater. Chem. Phys. 133 (2012) 992–997.
[13] J. Wang, Y. Hernandez, M. Lotya, J.N. Coleman, W.J. Blau, Broadband nonlinear optical response of graphene dispersions, Adv. Mater. 21 (2009) 2430–2435.
[14] T. Remyamol, H. John, P. Gopinath, Synthesis and nonlinear optical properties of reduced graphene oxide covalently functionalized with polyaniline, Carbon 59 (2013) 308–314.
[15] R.R. Nair, P. Blake, a.N. Grigorenko, K.S. Novoselov, T.J. Booth, T. Stauber, N.M.R. Peres, a.K. Geim, Fine structure constant defines visual transparency of graphene, Science 320 (2008) 1308.
[16] F. Bonaccorso, Z. Sun, T. Hasan, A.C. Ferrari, Graphene photonics and optoelectronics, Nat. Photon. 4 (2010) 611–622.
[17] D.A. Dikin, S. Stankovich, E.J. Zimney, R.D. Piner, G.H.B. Dommett, G. Evmenenko, S.T. Nguyen, R.S. Ruoff, Preparation and characterization of graphene oxide paper, Nature 448 (2007) 457–460.
[18] J. Zhu, Y. Li, Y. Chen, J. Wang, B. Zhang, J. Zhang, W.J. Blau, Graphene oxide covalently functionalized with zinc phthalocyanine for broadband optical limiting, Carbon. 49 (2011) 1900–1905.
[19] Y. Lin, J. Jin, M. Song, Preparation and characterisation of covalent polymer functionalized graphene oxide, J. Mater. Chem. 21 (2011) 3455.
[20] X. Zhao, X.Q. Yan, Q. Ma, J. Yao, X.L. Zhang, Z.B. Liu, J.G. Tian, Nonlinear optical and optical limiting properties of graphene hybrids covalently functionalized by phthalocyanine, Chem. Phys. Lett. 577 (2013) 62–67.
[21] L. Tao, B. Zhou, G. Bai, Y. Wang, S.F. Yu, S.P. Lau, Y.H. Tsang, J. Yao, D. Xu, Fabrication of covalently functionalized graphene oxide incorporated solid-state hybrid silica gel glasses and their improved nonlinear optical response, J. Phys. Chem. C 117 (2013) 23108–23116.
[22] F. Mammeri, J. Teyssandier, C. Connan, E. Le Bourhis, M.M. Chehimi, Mechanical properties of carbon nanotube–PMMA based hybrid coatings: the importance of surface chemistry, RSC Adv. 2 (2012) 2462–2468.
[23] C.J. Shearer, A.V. Ellis, J.G. Shapter, N.H. Voelcker, Chemically grafted carbon nanotube surface coverage gradients, Langmuir 26 (2010) 18468–18475.
[24] H. Zhou, C. Zhang, H. Li, Z. Du, Fabrication of silica nanoparticles on the surface of functionalized multi-walled carbon nanotubes, Carbon 49 (2011) 126–132.
[25] U. Khan, H. Porwal, A.O. Neill, P. May, J.N. Coleman, Solvent-exfoliated graphene at extremely high concentration solvent-exfoliated graphene at extremely high concentration, Langmuir 27 (2011) 9077–9082.
[26] D.W. Johnson, B.P. Dobson, K.S. Coleman, A manufacturing perspective on graphene dispersions, Curr. Opin. Colloid Interface Sci. 20 (2015) 367–382.
[27] S. Haar, M. El Gemayel, Y. Shin, G. Melinte, M.A. Squillaci, O. Ersen, C. Casiraghi, A. Ciesielski, P. Samorì, Enhancing the liquid-phase exfoliation of graphene in organic solvents upon addition of n-Octylbenzene, Sci. Rep. 5 (2015) 16684.
[28] B. Anand, A. Kaniyoor, S.S.S. Sai, R. Philip, S. Ramaprabhu, Enhanced optical limiting in functionalized hydrogen exfoliated graphene and its metal hybrids, J. Mater. Chem. C 1 (2013) 2773–2780.
[29] K.S. Novoselov, A.K. Geim, S.V. Morozov, D. Jiang, Y. Zhang, S.V. Dubonos, I.V. Grigorieva, A.A. Firsov, Electric field effect in atomically thin carbon films, Science 306 (2004) 666–669.
[30] A.A. Green, M.C. Hersam, Solution phase production of graphene with controlled thickness via density differentiation, Nano Lett. 9 (2009) 4031–4036.
[31] P. Eaton, P. Holmes, J. Yarwood, In situ and ex situ FTIR-ATR and Raman microscopic studies of organosilane hydrolysis and the effect of hydrolysis on silane

diffusion through a polymeric film, J. Appl. Polym. Sci. 82 (2001) 2016–2026.
[32] P.J. Launer, Infrared analysis of organosilicon compounds: spectra-structure correlations, Silicon Compd. Regist. Rev. (1987) 100–103.
[33] M. Hayyan, A. Abo-Hamad, M.A. AlSaadi, M.A. Hashim, Functionalization of graphene using deep eutectic solvents, Nanoscale Res. Lett. 10 (2015) 324.
[34] N. Liaros, K. Iliopoulos, M.M. Stylianakis, E. Koudoumas, S. Couris, Optical limiting action of few layered graphene oxide dispersed in different solvents, Opt. Mater. 36 (2013) 112–117.
[35] F.T. Johra, J.W. Lee, W.G. Jung, Facile and safe graphene preparation on solution based platform, J. Ind. Eng. Chem. 20 (2014) 2883–2887.
[36] E. Casero, C. Alonso, M.D. Petit-Domínguez, L. Vázquez, A.M. Parra-Alfambra, P. Merino, S. Álvarez-García, A. de Andrés, E. Suárez, F. Pariente, E. Lorenzo, Lactate biosensor based on a bionanocomposite composed of titanium oxide nanoparticles, photocatalytically reduced graphene, and lactate oxidase, Microchim. Acta. 181 (2014) 79–87.
[37] M. Sheik-bahae, A.A. Said, T. Wei, D.J. Hagan, E.W. Van Stryland, Sensitive measurement of optical nonlinearities using a single beam, IEEE J. Quant. Electron. 26 (1990) 760–769.
[38] J. Wang, Y. Chen, R. Li, H. Dong, Y. Ju, J. He, J. Fan, K. Wang, K.S. Liao, L. Zhang, S.a. Curran, W.J. Blau, Graphene and carbon nanotube polymer composites for laser protection, J. Inorg. Organomet. Polym. Mater. 21 (2011) 736–746.
[39] J. Wang, W.J. Blau, Solvent effect on optical limiting properties of single-walled carbon nanotube dispersions, J. Phys. Chem. C 112 (2008) 2298–2303.
[40] B. Zhao, B. Cao, W. Zhou, D. Li, W. Zhao, Nonlinear optical transmission of nanographene and its composites, J. Phys. Chem. C 114 (2010) 12517–12523.
[41] Y. Xu, Z. Liu, X. Zhang, Y. Wang, J. Tian, Y. Huang, Y. Ma, X. Zhang, Y. Chen, A graphene hybrid material covalently functionalized with porphyrin: synthesis and optical limiting property, Adv. Mater. 21 (2009) 1275–1279.
[42] M. Feng, H. Zhan, Y. Chen, Nonlinear optical and optical limiting properties of graphene families, Appl. Phys. Lett. 96 (2010) 033107.
[43] S. Bai, Q. Li, H. Zhang, X. Chen, S. Luo, H. Gong, Y. Yang, D. Zhao, M. Qiu, Large third-order nonlinear refractive index coefficient based on gold nanoparticle aggregate films, Appl. Phys. Lett. 107 (2015) 1–6.
[44] V.V. Bukin, S.V. Garnov, A.A. Malyutin, V.V. Strelkov, Femtosecond laser optical gas breakdown microplasma: the ionisation and postionisation dynamics, Quant. Electron. 37 (2008) 961–966.
[45] A. Wang, L. Long, W. Zhao, Y. Song, M.G. Humphrey, M.P. Cifuentes, X. Wu, Y. Fu, D. Zhang, X. Li, C. Zhang, Increased optical nonlinearities of graphene nanohybrids covalently functionalized by axially-coordinated porphyrins, Carbon 53 (2013) 327–338.
[46] Y. Liu, J. Zhou, X. Zhang, Z. Liu, X. Wan, J. Tian, T. Wang, Y. Chen, Synthesis, characterization and optical limiting property of covalently oligothiophene-functionalized graphene material, Carbon 47 (2009) 3113–3121.
[47] P.P. Kiran, D.R. Reddy, A.K. Dharmadhikari, B.G. Maiya, G.R. Kumar, D.N. Rao, Contribution of two-photon and excited state absorption in “axial-bonding” type hybrid porphyrin arrays under resonant electronic excitation, Chem. Phys. Lett. 418 (2006) 442–447.
[48] Z. Liu, Y. Wang, X. Zhang, Y. Xu, Y. Chen, J. Tian, Nonlinear optical properties of graphene oxide in nanosecond and picosecond regimes, Appl. Phys. Lett. 94 (2009) 1–4.